Optical properties and magnetic field-induced phase transitions in the ferroelectric state of $Ni_3V_2O_8$

R. C. Rai,[1] J. Cao,[1] S. Brown,[1] J. L. Musfeldt,[1,*] D. Kasinathan,[2]
D. J. Singh,[3] G. Lawes,[4] N. Rogado,[5] R. J. Cava,[6] and X. Wei[7]

[1]*Department of Chemistry, University of Tennessee, Knoxville, TN 37996*
[2]*Department of Physics, University of California Davis, Davis, CA 95616*
[3]*Materials Science and Technology Division, Oak Ridge National Laboratory, Oak Ridge,TN 37831-6032*
[4]*Department of Physics, Wayne State University, Detroit, MI 48201*
[5]*DuPont Central Research and Development, Experimental Station, Wilmington, DE 19880-0328*
[6]*Department of Chemistry and Princeton Materials Institute, Princeton University, Princeton, NJ 08544*
[7]*National High Magnetic Field Laboratory, Florida State University, Tallahassee, Florida 32310*

We use a combination of optical spectra, first principles calculations, and energy dependent magneto-optical measurements to elucidate the electronic structure and to study the phase diagram of $Ni_3V_2O_8$. We find a remarkable interplay of magnetic field and optical properties that reveals additional high magnetic field phases and an unexpected electronic structure which we associate with the strong magneto-dielectric couplings in this material over a wide energy range. Specifically, we observed several prominent magneto-dielectric effects that derive from changes in crystal field environment around Ni spine and cross-tie centers. This effect is consistent with a field-induced modification of local structure. Symmetry-breaking effects are also evident with temperature. We find $Ni_3V_2O_8$ to be an intermediate gap, local moment band insulator. This electronic structure is particularly favorable for magneto-dielectric couplings, because the material is not subject to the spin charge separation characteristic of strongly correlated large gap Mott insulators, while at the same time remaining a magnetic insulator independent of the particular spin order and temperature.

PACS numbers: 75.80.+q, 78.20.Ls, 71.20.Be,75.30.Et

I. INTRODUCTION

$Ni_3V_2O_8$ is a particularly interesting magnetic material,[1,2,3,4,5] both because of its unusual structure, which provides an example of a spin 1 system on a Kagomé staircase lattice, and because of the rich variety of magnetic and structural phases that are stabilized under different conditions. One especially interesting feature is the occurrence of a magnetic, ferroelectric phase as a function of temperature and magnetic field. More generally, coupled magnetic and electric degrees of freedom, flexible lattices, and magnetic frustration in multiferroics can result in cascades of coupled magnetic and dielectric transitions.[6,7,8,9,10,11,12,13] The recent report[10] of colossal low frequency (1 kHz) magneto-dielectric effects in inhomogeneously mixed-valent $DyMn_2O_5$ is especially important, because it illustrates that sizable dielectric contrast can be achieved by physical tuning through an unusual commensurate-incommensurate magnetic transition and is facilitated by a soft lattice. The 300 K low-frequency magneto-dielectric effect in mixed-valent $LuFe_2O_4$ has also attracted attention due to the very low magnetic fields needed to achieve dielectric contrast.[14] $Ni_3V_2O_8$ is another system where the temperature and field dependence of the spontaneous polarization shows a strong coupling between magnetic and ferroelectric order.[3,4,5] This coexistence is unusual and appears only when certain symmetry conditions are fulfilled.[3] That the effect can be controlled with an external magnetic field makes it attractive for device applications. Based upon our previous work with inhomogeneously mixed-valent $K_2V_3O_8$,[15] the significant coupling between spin, lattice, and charge degrees of freedom make $Ni_3V_2O_8$ an excellent candidate for discovery of higher energy magneto-dielectric effects.

Figure 1(a) shows the orthorhombic (Cmca) crystal structure of $Ni_3V_2O_8$. It consists of Kagomé layers of edge sharing NiO_6 octahedra separated by nonmagnetic VO_4 tetrahedra. $Ni_3V_2O_8$ is considered to be a Kagomé staircase compound due to buckling of the lattice perpendicular to the a axis. There are two distinct types of Ni^{2+} ($S = 1$) centers, which we refer to as "spine" and "cross-tie" sites. The "spine" sites run along the a axis. A view of the Kagomé staircase showing only the Ni atoms is displayed in Fig. 1(b). Note that the spine and

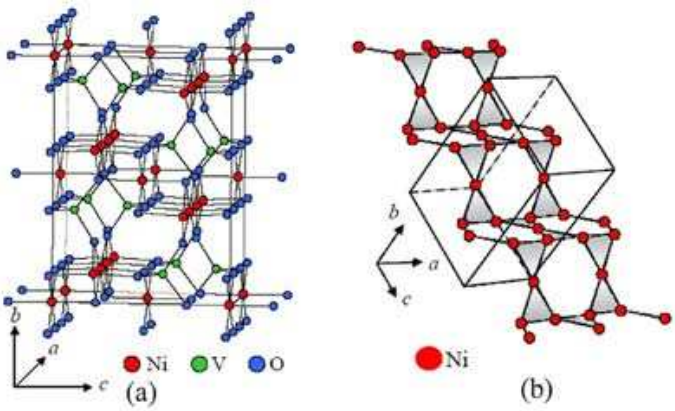

FIG. 1: (Color online) (a) Crystal structure of $Ni_3V_2O_8$. (b) View of Kagomé staircase showing only the Ni atoms.

cross-tie sites have very different local symmetries. The spin ordering arrangements in $Ni_3V_2O_8$ have been extensively investigated by neutron scattering and derive from various local and long range exchange, spin anisotropy, Dzyaloshinskii-Moriya, dipolar, and frustration effects.[5] The H-T phase diagram (for $H\|b$) is shown in Fig. 2(b). Two incommensurate phases are observed below the paramagnetic phase (PM). HTI is the (longitudinal) high temperature incommensurate phase, and LTI is the (spiral) low temperature incommensurate phase. The latter displays ferroelectricity. Commensurate canted antiferromagnetism is observed in the C phase.

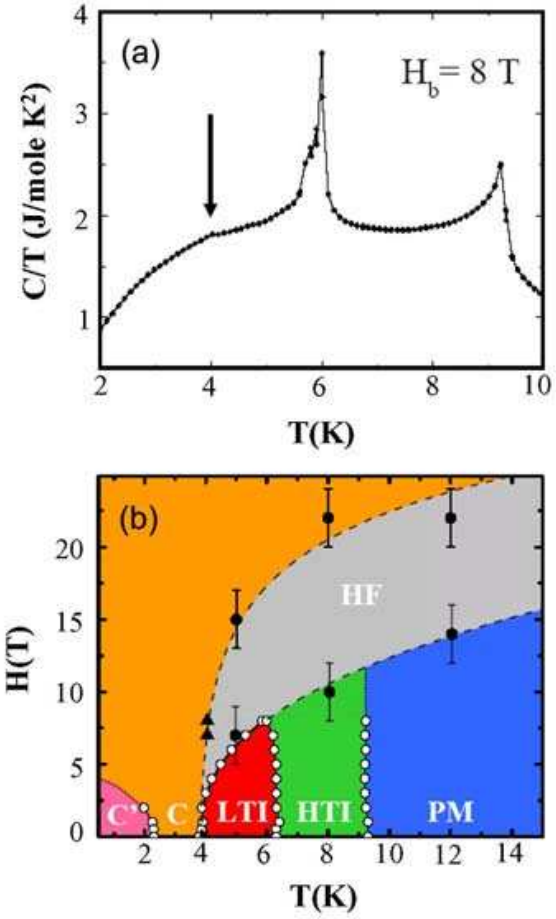

FIG. 2: (Color online) (a) Specific heat of $Ni_3V_2O_8$ as a function of temperature at $H = 8$ T. The arrow indicates a proposed phase transition temperature. (b) H-T phase diagram of $Ni_3V_2O_8$ for $H\|b$ with additional data points extracted from specific heat (solid triangles) and magneto-optical measurements (solid circles). Solid lines are discussed in the text and the dashed line is a guide to the eye. A new high field (HF) phase is also indicated.

Here we use a combination of optical spectroscopy, first principles calculations, and energy dependent magneto-optical measurements to elucidate the electronic structure and to study the phase diagram of $Ni_3V_2O_8$. We find a remarkable interplay of magnetic field and optical properties that reveals additional high magnetic field phases and an unexpected electronic structure which we associate with the strong magneto-dielectric couplings in this material over a wide energy range. Specifically, we observed several prominent magneto-dielectric effects that derive from changes in crystal field environment around Ni spine and cross-tie centers. This effect is consistent with a field-induced modification of local structure. Symmetry-breaking effects are also evident with temperature. Even though both $Ni_3V_2O_8$ and the prototypical Mott insulator NiO are based on Ni^{2+} ions octahedrally coordinated by O with similar bond lengths, we show that the basic electronic structures of these two materials are very different. NiO has a large band gap and local moments that derive from strong Coulomb interactions and separation of spin and charge degrees of freedom. This separation is theoretically interesting but disadvantageous if one wants to promote coupling effects. The Slater insulator is at the opposite extreme. Here, a small band gap is present in the ground state, but it is a direct result of a specific spin ordering. In contrast, we find $Ni_3V_2O_8$ to be an intermediate gap, local moment band insulator. This electronic structure is particularly favorable for magneto-dielectric couplings, because the material is not subject to the spin charge separation characteristic of strongly correlated large gap Mott insulators, while at the same time remaining a magnetic insulator independent of the particular spin order and temperature.

II. METHODS

A. Crystal Growth

The $Ni_3V_2O_8$ single crystal samples were prepared from a BaO-V_2O_5 flux. The crystals used for these measurements were grown as platelets, with their largest faces (a few square millimeters) perpendicular to the crystallographic b axis.

B. Spectroscopic Investigations

Near normal ac-plane reflectance of $Ni_3V_2O_8$ was measured over a wide energy range (3.7 meV - 6.5 eV) using several different spectrometers including a Bruker 113 V Fourier transform infrared spectrometer, a Bruker Equinox 55 Fourier transform infrared spectrometer equipped with an infrared microscope, and a Perkin Elmer Lambda 900 grating spectrometer, as described previously.[16] The spectral resolution was 2 cm^{-1} in the far and middle-infrared and 2 nm in the near-infrared, visible, and near-ultraviolet. Optical conductivity was calculated by a Kramers-Kronig analysis of the measured reflectance.[17] An open flow cryostat provided temperature control.

The magneto-optical properties of $Ni_3V_2O_8$ were investigated between 0.75 and 4.1 eV using a 3/4 m grating spectrometer equipped with InGaAs and CCD detectors and a 33 T resistive magnet at the National High Magnetic Field Laboratory (NHMFL), in Tallahassee, FL. 150, 300, and 600 line/mm gratings were used, as appropriate. Experiments were performed with polarized light ($E\|a$ and $E\|c$) in the temperature range between 4.2 and 15 K for applied magnetic fields up to 30 T ($H\|b$). With light shining on the sample, we estimate that the base temperature was ∼5.0 K. The field-induced changes in the measured reflectance were studied by taking the ratio of the reflectance at each field with the reflectance at zero field, i.e., [R(H)/R(H = 0 T)]. This normalized response is a sensitive way to view the field-induced optical changes.[18] Since $\epsilon(E) = \epsilon_1(E) + i\epsilon_2(E) = \epsilon_1(E) + \frac{4\pi i}{\omega}\sigma_1(E)$, it is clear that the field-induced changes in reflectance translate into finite energy magneto-dielectric effects. To obtain the 30 T optical conductivity (σ_1) and dielectric response (ϵ_1), we renormalized the zero-field absolute reflectance with the high-field reflectance ratios, and recalculated σ_1 and ϵ_1 using Kramers-Kronig techniques.[15,17]

C. Electronic Structure Calculations

The calculations were done with the experimental crystal structure[1] using the general potential linearized augmented planewave (LAPW) method, with local orbitals,[19,20] as implemented in the WIEN2K program.[21] The augmented planewave plus local orbital extension was used for the O s and p states, the metal d states and the semi-core levels.[22] The valence states were treated in a scalar relativistic approximation, while the core states were treated relativistically. The calculations were done self-consistently using well converged basis sets and zone samplings based on 144 **k**-points in the irreducible wedge. A more dense mesh of 1200 **k**-points was used for the calculations of the optical conductivity. The LAPW sphere radii were 1.8, 1.7 and 1.5 a_0 for Ni, V and O, respectively. Calculations were done in the local spin density approximation (LSDA) and the LDA+U method. For the LDA+U calculations, we used values of U ranging from 5 eV to 7 eV on the Ni sites. The results shown are for U = 5 eV.[23]

III. RESULTS AND DISCUSSION

A. Optical and Electronic Properties of $Ni_3V_2O_8$

Figure 3(a) displays the polarized optical conductivity of $Ni_3V_2O_8$ in the PM phase at 300 and 12 K. The spectra show directionally dependent vibrational and electronic excitations with an optical energy gap of ∼0.35 eV. Based on our electronic structure calculations (discussed in detail below) and comparison with chemically

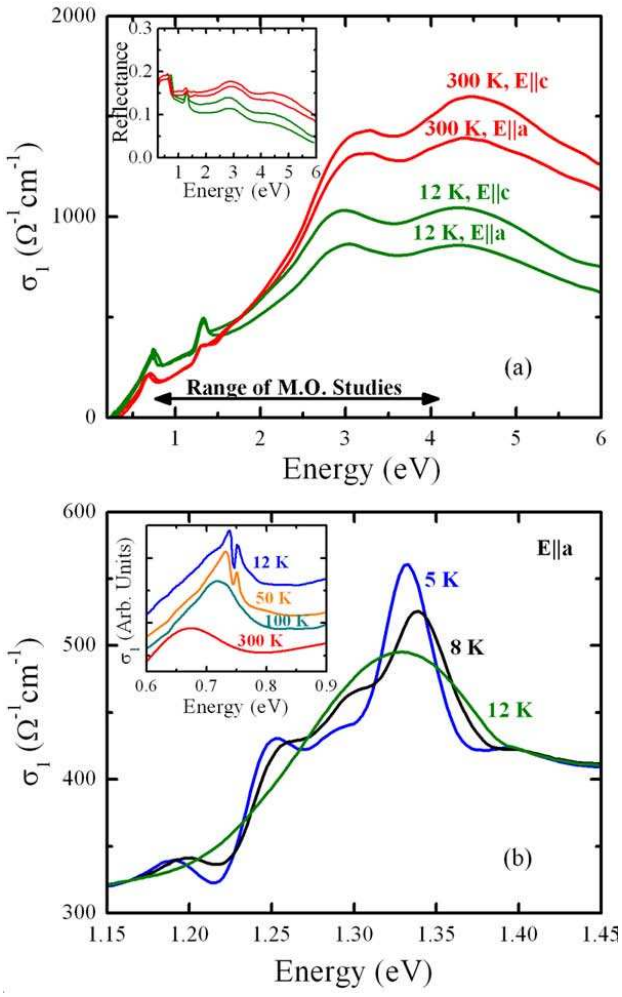

FIG. 3: (Color online) (a) Polarized optical conductivity of $Ni_3V_2O_8$ at 300 and 12 K, extracted from reflectance measurements (inset) by a Kramers-Kronig analysis. The energy range of our magneto-optical measurements is indicated by the arrow (0.75 - 4.1 eV). (b) A close-up view of the $E\|a$ optical conductivity at 12, 8, and 5 K, corresponding to Ni (spine) d to d on-site excitations. Inset shows a close-up view of Ni (cross-tie) d to d on-site excitations at T = 300, 100, 50, and 12 K, respectively. These curves are offset for clarity.

similar Ni-containing compounds,[24,25,26,27] we assign the excitations centered near ∼0.75 and ∼1.35 eV to Ni d to d on-site excitations in the minority spin channel on cross-tie and spine sites, respectively. These excitations are optically allowed due to the modest hybridization between the Ni d and O p states. We assign the ∼3.0 eV feature in the optical conductivity spectrum to a combination of O 2p to Ni 3d and O 2p to V 3d charge transfer excitations. The ∼4.4 eV feature derives from O 2p to V 3d charge transfer excitations.

Transition metal d to d on-site excitations are sensitive indicators of the local crystal field environment. Figure 3(b) shows a close-up view of the Ni (spine) d to d on-site excitations in the $E\|a$ optical conductivity at 12, 8, and 5 K. This structure is broad and featureless in the

PM phase (12 K), but it splits into at least four different components at 8 K (HTI phase). The splitting becomes more pronounced at 5 K (LTI phase). This splitting is due to a local structure distortion around the Ni center with decreasing temperature and demonstrates that the NiO_6 environment is different in the PM, HTI, and LTI phases. Although it is at the limit of our detector range, the trailing edge of the ∼0.75 feature also displays splitting below 12 K (not shown).[28] Interestingly, the Ni (cross-tie) d to d on-site excitation also shows a notch-like structure that develops between 100 and 50 K (inset of Fig. 3(b)), indicating that a weak structural distortion in the cross-tie direction precedes the cascade of low temperature magnetic phases. Anomalous intermediate temperature phonon shifts have also been reported in the RMn_2O_5 (R = Bi, Eu, Dy) family of frustrated multiferroics.[29]

B. Electronic Structure Calculations of $Ni_3V_2O_8$

As mentioned above, there are two nonequivalent Ni sites in the unit cell, a spine site (4 atoms per cell, denoted Ni2 in the following) and a cross-link site (2 atoms per cell, denoted Ni1). As mentioned, $Ni_3V_2O_8$ is a local moment magnet with a complex magnetic phase diagram. To assign the peaks in the optical spectrum, we did calculations for two magnetic structures: (1) all spins on each Ni sublattice aligned ferromagnetically, but with the two sublattices opposite to each other (denoted FiM, in the following) and (2) a ferromagnetic ordering (FM). In the LSDA, the FiM ordering had lower energy by 7 meV per formula unit (note that there are two formula units per cell). This shows an antiferromagnetic interaction between the two sublattices.

The calculated total and projected densities of states (DOS) for the FiM ordering are shown in Fig. 4 and Fig. 5, within the LSDA and the LDA+U (U = 5.0 eV) approximation, respectively. In addition to the U = 5 eV DOS shown, we did calculations for U = 6 eV and U = 7 eV (see below). Insulating behavior is found in both approximations. The gaps are E_g(LSDA) = 0.30 eV and E_g(LDA + U) = 1.90 eV. There are only relatively small changes in the O $2p$ bands between these two approximations. The O $2p$ valence bands extend from ∼ -6.5 eV to the valence band edge in the LSDA, and from ∼ -6.0 eV to the band edge in the LDA+U approximation. Wang and co-workers[30] investigated $Ni_3V_2O_8$ as a potential photocatalyst for water splitting using optical spectroscopy from 300 nm to 850 nm, and density functional calculations. However, they did not include spin-polarization in their band structure calculations, and this is needed to obtain the exchange splitting of the Ni d states. As a result, they obtained a metallic electronic structure with a high density of Ni d states at the Fermi energy in disagreement with experiment.

The compound is described as $Ni_3^{2+}V_2^{5+}O_8^{2-}$. As shown in the projected DOS, we find the V d bands well above

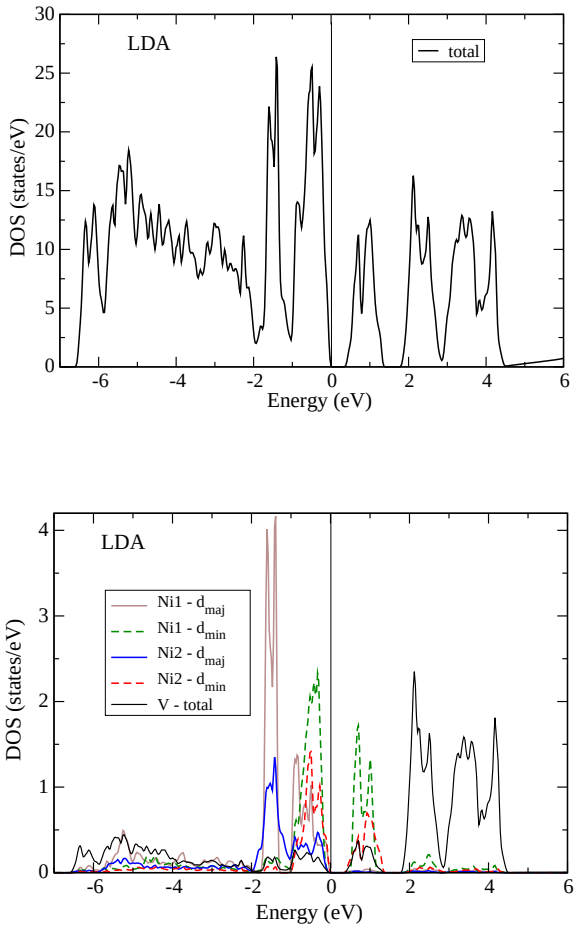

FIG. 4: (color online) Total (top) and projected DOS (bottom) as obtained with the LSDA for the FiM ordering (see text). The total DOS is on a per formula unit spin basis. The projections are onto the LAPW spheres, and are given per atom.

valence bands in both the LSDA and LDA+U calculations (from ∼ 2 eV to ∼ 5 eV, relative to the valence band edge), in agreement with this ionic model. In all calculations, we find integer spin magnetizations of 2 μ_B per Ni ion, as expected for Ni^{2+}. In the crystal field, the main Ni d splitting is due to the local coordination, which gives a lower 3-fold degenerate t_{2g} and a higher two-fold degenerate e_g manifold per spin. The Ni d bands are already very narrow in the LSDA. This is the reason for the clean gap. In the FM case, the band gap E_g is reduced by only 0.11 eV relative to the FiM case. Presumably, antiferromagnetism within the individual sublattices would narrow the bands further and increase E_g relative to the FiM ordering. Thus, already at the LSDA level, $Ni_3V_2O_8$ is a local moment insulator. The majority spin Ni d levels are centered at -1.7 eV (t_{2g}) and -0.6 eV (e_g), for both Ni sites. The corresponding minority spin levels are centered at -0.4 eV (t_{2g}) and 0.8 eV (e_g).

The main difference between the LSDA and LDA+U

electronic structure is in the position of the Ni d bands. The majority spin Ni manifolds are shifted deep into the valence band. These are centered at $\sim$ -5.5 eV (t_{2g}) and $\sim$ -2.5 eV (e_g). The minority spin states are split apart by the Coulomb interaction and are now centered at $\sim$ -1 eV (t_{2g}) and $\sim$ 2.5 eV (e_g). For this value of U the conduction band edge onset derives from both V d and Ni d states. Calculations with $U = 6$ eV and $U = 7$ eV increase the differences from the LSDA, pushing the Ni d conduction band onset above the V d onset and driving the occupied Ni d manifolds deeper into the O p bands.

The calculated LSDA and LDA+U optical spectra for FiM ordering are shown in Fig. 6. Besides the larger LDA+U band gap, the shapes of the spectra are very different. In the LSDA the onset has both Ni d - Ni d and charge transfer character. The first structure just above 1 eV is due to the structure in the Ni d to Ni d excitations. It contains two peaks. The Ni1 (cross-link) site has a lower primary crystal field splitting than the Ni2 (spine) site, as may be seen from the projected DOS. Therefore, the lower energy peak comes more from the Ni1 and the higher peak from the Ni2. The second main structure above 2 eV, which is weaker, is of mainly charge transfer character involving Ni and V, and the onset starting at 3 eV is mainly of charge transfer character into the V d bands. In the LDA+U case the spectrum starts at $\sim$ 2 eV and is dominated throughout by charge transfer excitations.

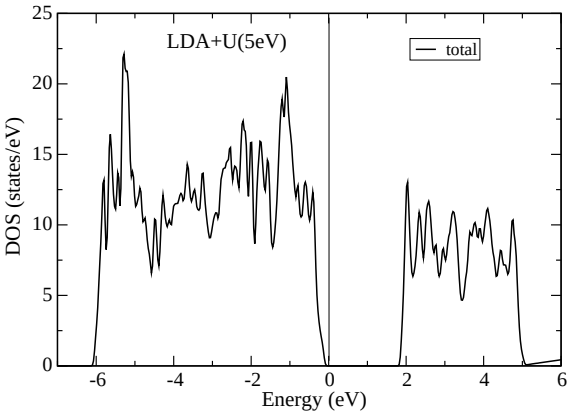

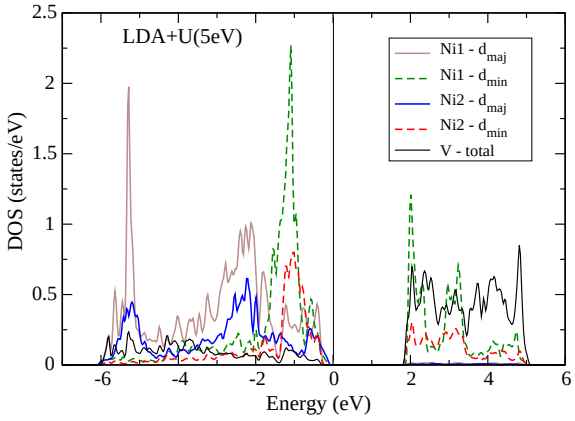

FIG. 5: (color online) Total (top) and projected DOS (bottom), as in Fig. 4, but with the LDA+U method, $U = 5$ eV.

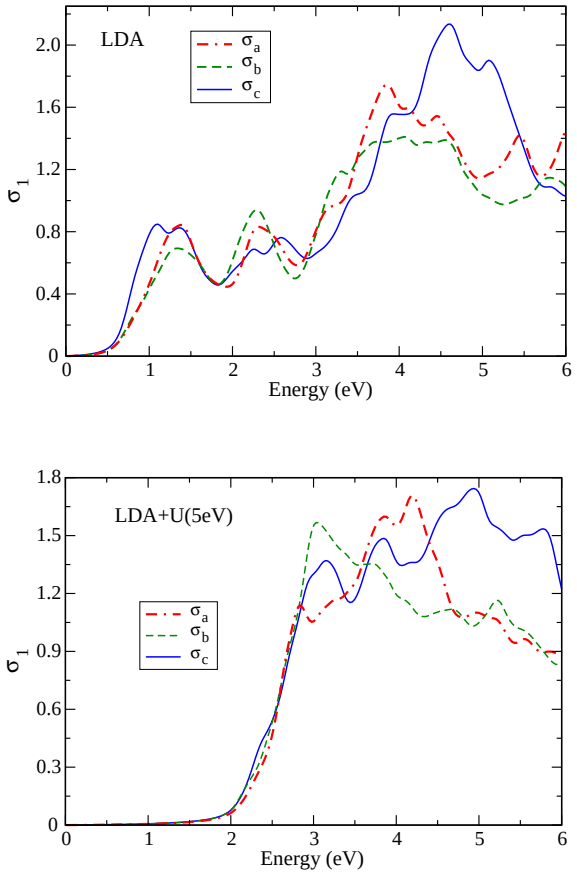

FIG. 6: Real part of the optical conductivity within the LSDA (top) and LDA+U, $U = 5$ eV (bottom), for $Ni_3V_2O_8$ with the FiM ordering. A 0.1 eV broadening was applied. Two definitions of the crystallographic axes are in literature. We use the one where $a = 5.936$ Å, $b = 11.420$ Å, and $c = 8.240$ Å.[1]

The LSDA spectrum is clearly in better accord with the experimental spectrum than the LDA+U spectrum, both in terms of the gap and in terms of the peak structure. The main differences between LSDA and experiment are in the region of the second peak (above 2 eV) and in the onset of the O $2p$ to V d charge transfer excitations. Considering that V is in a d^0 configuration, the underestimate of this gap is not surprising and presumably reflects just the generic LDA band gap underestimation, which is seen in other d^0 oxides. The relatively good agreement of the LSDA Ni d position and the fundamental gap with experiment is, however, unexpected and deserves comment.

NiO, which like $Ni_3V_2O_8$, has Ni^{2+}, six-fold coordi-

nated by O, is a prototypical Mott insulator. LSDA calculations for antiferromagnetic NiO show a small band gap and features in the valence band dispersions in accord with experiment.[31] However, the gap obtained is much smaller than the experimental gap of $\sim$ 4 eV, and furthermore it is dependent on the specific magnetic ordering. Furthermore, the LSDA gap of NiO is of incorrect *d*-*d* character rather than the charge transfer character observed in experiment.[24,32] This shows an essential role for beyond LSDA Coulomb correlations in describing the electronic structure of NiO. Various methods, including the LDA+U approximation, for incorporating these have been developed and tested using NiO.[33,34,35,36,37,38,39,40,41] As mentioned, NiO and $Ni_3V_2O_8$ both have Ni^{2+} in approximately octahedral O cages. In NiO, the Ni band width is larger than in $Ni_3V_2O_8$, which explains why the LSDA is able to produce local moment insulating behavior in this compound but not in NiO. The narrower bands in $Ni_3V_2O_8$ are related to the bonding topology. In NiO, the O are six fold coordinated with 90° and straight 180° bonds. $Ni_3V_2O_8$ has lower O coordination and bent bonds. In metals, the criterion for dividing strongly correlated materials from band metals involves U_s/W, where W is the band width and U_s is the screened Coulomb potential, where the "s" is simply to distinguish this parameter from the U used in the LDA+U approximation. In general, Mott insulators derived from metals with U_s/W cannot be described in the LSDA and require the use of the LDA+U approximation or more sophisticated approaches, while materials with weaker correlations are often better described in LSDA than in LDA+U calculation. Since the band width of $Ni_3V_2O_8$ is not larger than that of NiO, the implication of our results is that the effective screened Coulomb interaction U_s on at least one of the Ni sites is sufficiently lower than in NiO to cross-over from strongly correlated Mott insulator to band insulator. We speculate that this could be due to the lower cation coordination of O^{2-} in $Ni_3V_2O_8$. Specifically, in NiO, six Ni atoms compete for bonding with each O (two per O p orbital). The average Ni-O bond length in $Ni_3V_2O_8$ is $\sim$ 0.03 Å shorter than in NiO, consistent with this from the bond valence point of view.[42] This is not the case in $Ni_3V_2O_8$, which may enable the O cage to more effectively screen the bare U. As mentioned, we find $Ni_3V_2O_8$ to be a local moment insulator with weak sensitivity of the band structure to the magnetic order at the LDA level.

Figure 7 shows the calculated optical spectra for FM ordering. As may be seen it is qualitatively similar in structure to that of FiM ordering, but shows noticeable quantitative differences. Most notably there are changes in the shape of the low energy Ni d - d peak, a suppression of the second peak and changes in the shape of the onset of the higher energy charge transfer onset. Since neither the FiM or the FM ordering are the ground state ordering, these differences should be viewed as indicating the errors on our calculation when comparing with the experimental zero field spectrum. They also support the

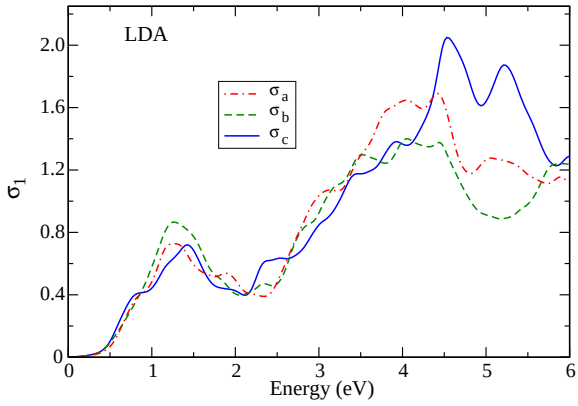

FIG. 7: Real part of the optical conductivity within the LSDA, as in Fig. 6, but with FM ordering.

experimental finding of substantial magnetochromic effects in this material. Interestingly, we find considerable orientation dependence of the magnetochromic effects in this material.

Optical excitations are charge excitations. Since Hubbard correlations generally harden charge degrees of freedom leading to spin charge separation one may expect stronger charge spin coupling, and perhaps stronger magnetochromic effects in less correlated materials. This is also relevant to the magnetoelectric coupling observed in $Ni_3V_2O_8$, since strong Coulomb correlations, if present, would reduce the spin-lattice coupling, so that while ferroelectricity would still be induced by the incommensurate magnetic order, it would be weaker due to reduced coupling. Based on our results, we find that the Ni sites in $Ni_3V_2O_8$ are not subject to strong correlations, and this underlies the substantial magnetochromic effects seen in this material.

C. Magneto-Optical Properties of $Ni_3V_2O_8$

Figure 8(a) and (b) shows the reflectance ratio of $Ni_3V_2O_8$, R(H)/R(H=0 T), at 5 K. Rich field-induced changes in reflectance are observed over the full energy range in both polarizations. The most significant modifications are near 0.75 and 1.35 eV, providing a preview of the physical origin of the field-induced effects. Based on the aforementioned positions of the magneto-optical features, we attribute these changes to field-induced modifications of Ni (cross-tie) d to d and Ni (spine) d to d on-site excitations. At 30 T, the reflectance deviates from unity by $\pm$15% near 1.35 eV. On the other hand, reflectance changes in the visible range (centered at $\sim$2.2, 2.6, and 3.3 eV) are much broader and more modest in size (up to $\sim$4% for 30 T at 5 K), similar in magnitude to "magnetochromic effects" reported on other complex materials.[15,25,43,44] These features can be attributed to field-induced changes in O 2p to Ni 3d and O 2p to V 3d charge transfer excitations.

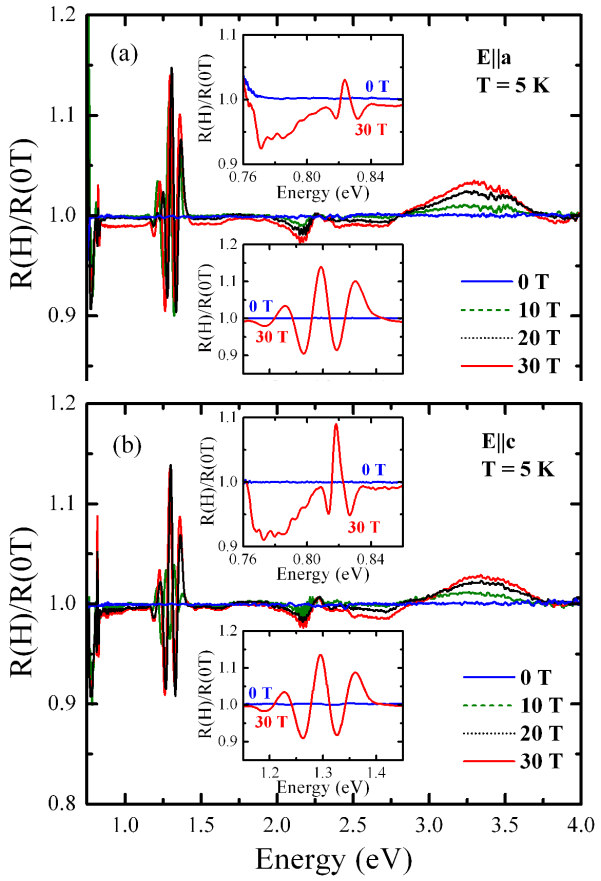

FIG. 8: (Color online) The normalized magneto-optical response, R(H)/R(H=0 T), of $Ni_3V_2O_8$ in an applied magnetic field ($H\|b$) from 0 to 30 T at 5 K (a) for light polarized along the a direction. (b) for light polarized along the c direction. The insets show close-up views of the magneto-optical response near the Ni (cross-tie) and Ni (spine) d to d on-site excitations. Data were taken in 2 T steps, but only representative curves are displayed for clarity.

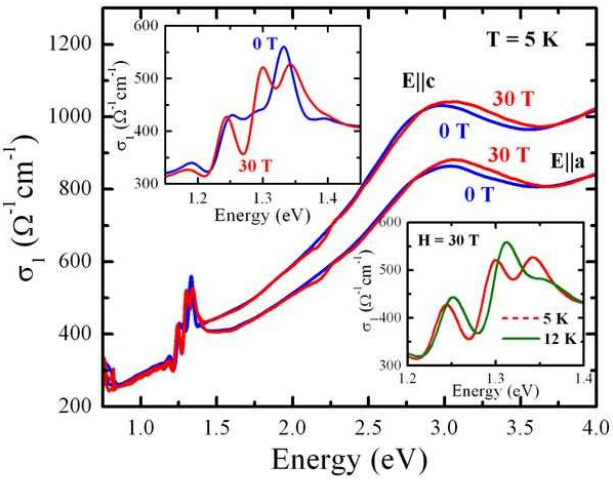

FIG. 9: (Color online) Polarized optical conductivity of $Ni_3V_2O_8$ at 5 K for H = 0 and 30 T ($H\|b$). $E\|a$ and $E\|c$ polarizations are indicated by dashed and solid lines, respectively. The upper inset shows a close-up view of the energy region near the Ni (spine) d to d on-site excitation for H = 0 and 30 T. The lower inset shows a close-up view of the Ni (spine) d to d on-site excitation for T = 12 and 5 K at 30 T.

It is desirable to correlate field-induced reflectance ratio changes with the dispersive and lossy response of the material. Figure 9 displays the polarized optical conductivity of $Ni_3V_2O_8$ at 5 K at 0 and 30 T ($H\|b$), extracted from a combination of absolute reflectance measurements, the reflectance ratio data of Fig. 8(a) and (b), and a Kramers-Kronig analysis and calculation of the optical constants. From the optical conductivity, we can immediately confirm that the aforementioned magneto-optical effects correspond to field-induced modifications of the Ni (cross-tie) d to d, Ni (spine) d to d on-site excitations, and O 2p to Ni 3d and O 2p to V 3d charge transfer excitations. The insets of Fig. 9 show close-up views of the ∼1.35 eV Ni on-site excitation splittings that point toward a field-induced local distortion of the NiO_6 octahedra.[28] As mentioned previously, these Ni d to d excitations are allowed because oxygen hybridization modifies the matrix elements. The charge transfer excitation centered at ∼3.0 eV also broadens and blueshifts with applied field, and a small "notch" develops at ∼ 2.2 eV. The reflectance ratio trends discussed above also capture important dispersive effects. Figure 10(a) shows the high energy magneto-dielectric response of $Ni_3V_2O_8$ at 5 K for $E\|a$. Although dielectric contrast ($\Delta\epsilon_1/\epsilon_1$) is subtle in the majority of the visible region (Fig. 10(c)), the applied field changes the dielectric constant significantly near the Ni d to d on-site excitations (inset, Fig. 10(a), and Fig. 10(b)). At some energies, dielectric contrast is on the order of 15% (Fig. 10(b)). These results demonstrate that magneto-dielectric effects are not confined to kHz frequencies and that the response may be tunable. Both aspects may be useful for device applications (for instance, magnetically controlled ferroelectric memory). This remarkable interplay between the magnetic field and optical constants of $Ni_3V_2O_8$ seems to be facilitated by the fact that this material is in the intermediate coupling regime, as discussed below.

Comparison of the reflectance ratio data in the upper insets of Fig. 8(a) and (b) provides insight into possible magnetoeleastic coupling in $Ni_3V_2O_8$. The structure centered at ∼0.83 eV is large in the c (cross-tie) direction, whereas it is much smaller along the a (spine) direction. It grows quickly with applied field. The splitting of this structure (∼12 meV (97 cm^{-1})) corresponds to a vibrational energy scale. Candidates for possible coupling might therefore include the displacement of Ni (cross-tie) atoms or a low-frequency O-Ni-O bending mode. In the presence of a soft lattice, magnetoelastic coupling may lead to a local distortion of the NiO_6 octahedra. Note that the PM phase of a frustrated magnetic system often displays significant spin correlations.[29] The PM phase in $Ni_3V_2O_8$ may be similar, consistent with

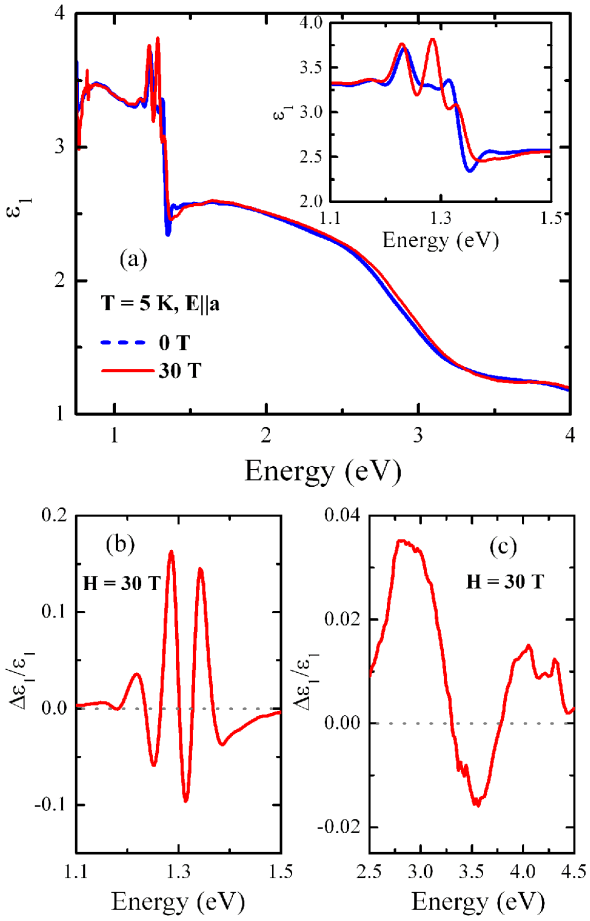

FIG. 10: (Color online) (a) Dielectric constant of $Ni_3V_2O_8$ at 5 K for light polarized along the a direction for H = 0 and 30 T ($H\|b$). The inset shows a close-up view of the energy region near the Ni (spine) d to d on-site excitation. Close-up views of the high-energy dielectric contrast, $\Delta\epsilon_1/\epsilon_1 = [\epsilon_1(E,H) - \epsilon_1(E,0)]/\epsilon_1(E,0)$, near (b) the Ni (spine) d to d on-site excitation and (c) the charge transfer excitations.

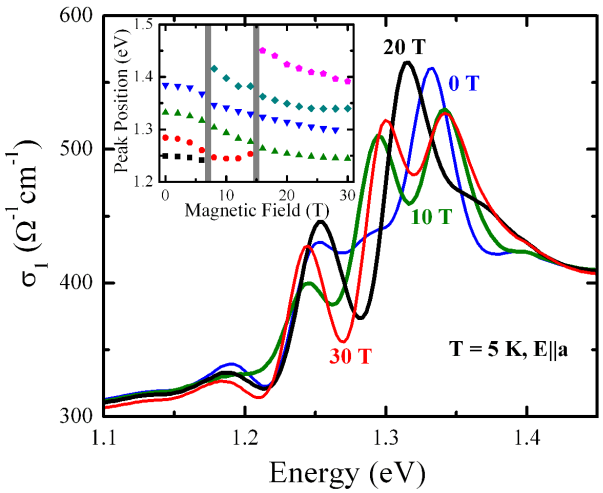

FIG. 11: (Color online) Polarized optical conductivity of $Ni_3V_2O_8$ at 5 K for H = 0, 10, 20, and 30 T ($H\|b$). The inset shows the peak position of fitted oscillators as a function of applied magnetic field. The shaded regions represent transition fields, from which the extended H-T phase diagram in Fig. 2(b) was generated.

the presence of magnetoelastic coupling. Direct measurements of high field vibrational properties of $Ni_3V_2O_8$ are clearly desirable. We note that spin-lattice coupling leads to structural distortions in the frustrated magnetic system $ZnCr_2O_4$.[45,46] Magnetoelastic coupling also plays an important role in geometrically frustrated magnetic systems such as $HoMnO_3$ and RMn_2O_5 (R = Tb, Ho, Dy).[7,8,10,29,47,48]

Spin-charge coupling in $Ni_3V_2O_8$ can be further investigated by quantifying the subtle changes in the Ni (spine) d to d on-site excitation with applied field. Figure 11 shows a close-up view of polarized optical conductivity of $Ni_3V_2O_8$ at 5 K for H = 0, 10, 20, and 30 T ($H\|b$). The effect of applied field is non-monotonic and correlates with changes in magnetic order. Peak fits, using four model oscillators, were used to elucidate these trends (inset, Fig. 11). The dependence of peak positions on the applied field clearly demonstrates an interplay between electronic and magnetic properties. For instance, at 5 K, the data shows discontinuities near 7 and 15 T, indicated by the grey shaded regions in the inset. These transition regions move to higher fields with increasing temperature. We note that the low field phase boundaries determined in this manner are in good overall agreement with the previously reported thermodynamic data. This optical properties work also allows us to follow the C/LTI phase boundary to higher fields, where it crosses over both the HTI and PM phases. Finally, these studies also identify a new "High Field" (HF) region, nestled between C and the cascade of LTI, HTI, and PM phases at higher temperature (Fig. 2(b)). Reexamination of previous specific heat measurements on $Ni_3V_2O_8$ are consistent with the presence of an additional weak transition for H = 8 T, as shown by the arrow in (Fig. 2(a)). A similar transition was also observed at H = 7 T.

As discussed in the Introduction, $Ni_3V_2O_8$ has a complex H-T phase diagram with several low field phases arising from the complex spin structures.[3,4] With the new transition fields extracted from the magneto-optical data at 5, 8, and 12 K (solid circles) and specific heat data (solid triangles), we extended the H-T phase diagram of Ref.[4] for $H\|b$, as shown in Fig. 2(b). We used the combined optical and specific heat data to establish the boundaries for the newly identified high field phase. It has been predicted[4] that the phase boundary for the LTI phase should be quadratic in H, so that $(T_c(H)\text{-}T_c(0)) \sim H^2$. Rather than this quadratic dependence, we find that this phase boundary can be fit by $(T_c(H)\text{-}T_c(0)) \sim H^{2.5}$. This fit is shown by the lower solid line in Fig. 2(b). The origins for this discrepancy are unclear at this time. The upper solid line in Fig. 2(b) is a guide to the

eye for the high field (HF) phase boundary. To the best of our knowledge, there has been no discussion of any possible functional form that might apply to this boundary. Combined magnetization and specific heat measurements in high magnetic fields will be required to precisely determine the magnetic field dependence of both phase boundary lines, which in turn will provide mechanistic information on the underlying magnetic transitions. Addition of the new data points from optical and specific heat studies also demonstrates the existence of a new HF phase that overlays the other low field regions. Neutron experiments are needed to assess magnetic order in the HF phase.

In addition to the 5 K (LTI phase) data discussed in detail here, we also collected full data sets in the HTI and PM phases of $Ni_3V_2O_8$. Strong magneto-optical effects were observed at both 8 and 12 K. As shown in Fig. 12, the magneto-optical effects in the PM phase are qualitatively similar to those of the LTI and HTI (not shown) phases, although the overall size of the field-induced modification is smaller. This result demonstrates that an applied field induces a local structural distortion around the Ni sites in all of the low temperature phases. In otherwords, the field-induced distortion is not unique to the LTI (ferroelectric) phase with spontaneous polarization. To support this claim, we refer the reader to the inset of Fig. 12(b)), where the zero-field ∼1.35 eV excitation is featureless. An applied field splits this structure into several distinct components, demonstrating the field-induced distortion of the Ni (spine) crystal field environment even in the PM phase.

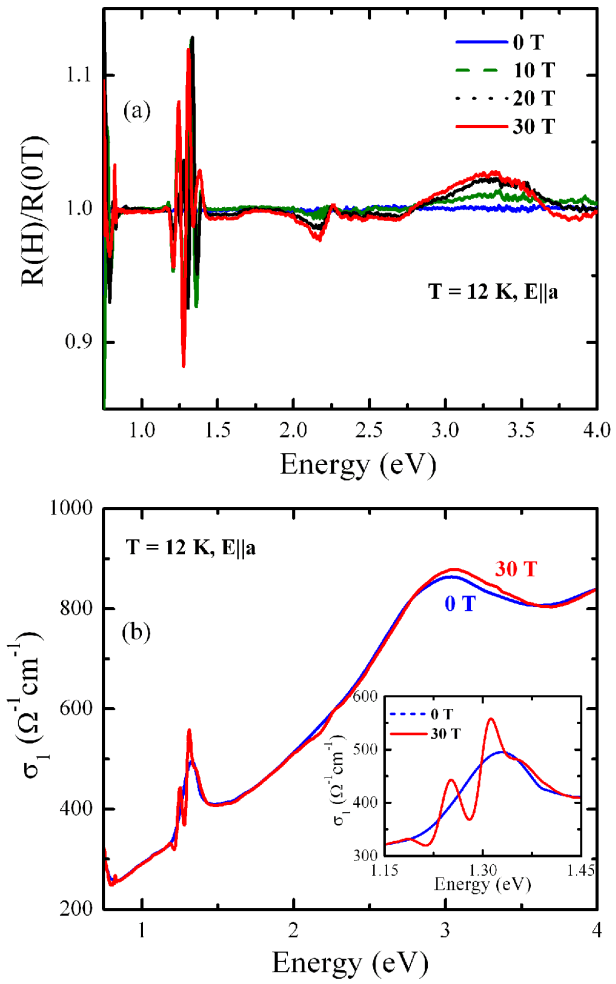

FIG. 12: (Color online) (a) The normalized magneto-optical response, R(H)/R(H=0 T), of $Ni_3V_2O_8$ in an applied magnetic field ($H\|b$) from 0 to 30 T at 12 K for light polarized along the a direction. (b) Polarized optical conductivity of $Ni_3V_2O_8$ at 12 K for H = 0 and 30 T ($H\|b$). Inset shows a close-up view of the magneto-optical response near the Ni (spine) d to d on-site excitation.

IV. CONCLUSION

We investigated the optical properties, electronic structure, and energy dependent magneto-optical response of $Ni_3V_2O_8$ to elucidate the electronic structure and to study the phase diagram. The spectra exhibit features centered at ∼0.75 and ∼1.35 eV that we assign as Ni (cross-tie and spine) d to d on-site excitations in the minority spin channel. O $2p$ to Ni $3d$ and O $2p$ to V $3d$ charge transfer excitations appear at higher energy. Extensive analysis of splitting patterns of the Ni (spine) d to d excitation in the PM, HTI, and LTI phases demonstrates that the local Ni environment is sensitive to magnetic order even at zero field. A splitting of Ni (cross-tie) d to d on-site excitation between 50 and 100 K also points toward a weak local structural distortion that precedes the cascade of low temperature magnetic phases. Although both $Ni_3V_2O_8$ and the prototypical Mott insulator NiO are based on Ni^{2+} ions octahedrally coordinated by O with similar bond lengths, the basic electronic structures of these two materials are very different. NiO has a large band gap and local moments that derive from strong Coulomb interactions and separation of spin and charge degrees of freedom, while, in contrast, we found $Ni_3V_2O_8$ to be an intermediate gap, local moment band insulator. This electronic structure is particularly favorable for magneto-dielectric coupling, because the material is not subject to the spin charge separation of the strongly correlated large gap Mott insulator, while at the same time, remaining a magnetic insulator independent of the particular spin order and temperature. The remarkable interplay of magnetic field and optical properties in $Ni_3V_2O_8$ reveals an additional high field phase and an unexpected electronic structure, which we associate with the strong magnetodielectric couplings in this material. We discovered several prominent magneto-optical effects that derive from changes in crystal field environment around Ni (spine and cross-tie) centers due to a field-induced modification of local structure of NiO_6. The magnetoelastic mechanism, responsible for the field-induced distortion of the NiO_6 building block unit, is active in the paramagnetic phase as well.

V. ACKNOWLEDGMENTS

Work at the University of Tennessee is supported by the Materials Science Division, Basic Energy Sciences, U.S. Department of Energy (DE-FG02-01ER45885). Research at ORNL is sponsored by the Division of Materials Sciences and Engineering, Office of Basic Energy Sciences, U.S. Department of Energy, under contract DE-AC05-00OR22725 with Oak Ridge National Laboratory, managed and operated by UT-Battelle, LLC. Work at UC Davis is supported by DOE grant DE-FG03-01ER45876. A portion of this research was performed at the NHMFL, which is supported by NSF Cooperation Agreement DMR-0084173 and by the State of Florida. Work at Princeton University is supported by NSF through the MRSEC program (NSF MRSEC grant DMR-9809483). We appreciate useful discussions with W. E. Pickett, and thank Q. Huang and M. Woodward for their assistance in preparing Fig. 1.

---

* Electronic address: musfeldt@utk.edu

[1] E. E. Sauerbrei, R. Faggiani, and C. Calvo, Acta Cryst. B **29**, 2304 (1973).

[2] N. Rogado, G. Lawes, D. A. Huse, A. P. Ramirez, and R. J. Cava, Solid State Commun. **124**, 229 (2002).

[3] G. Lawes, A. B. Harris, T. Kimura, N. Rogado, R. J. Cava, A. Aharony, O. Entin-Wohlman, T. Yildirim, M. Kenzelmann, C. Broholm, and A. P. Ramirez, Phys. Rev. Lett. **95**, 087205 (2005).

[4] G. Lawes, M. Kenzelmann, N. Rogado, K. H. Kim, G. A. Jorge, R. J. Cava, A. Aharony, O. Entin-Wohlman, A. B. Harris, T. Yildirim, Q. Z. Huang, S. Park, C. Broholm, and A. P. Ramirez, Phys. Rev. Lett. **93**, 247201 (2004).

[5] M. Kenzelmann, A. B. Harris, A. Aharony, O. Entin-Wohlman, T. Yildirim, Q. Huang, S. Park, G. Lawes, C. Broholm, N. Rogado, R. J. Cava, K. H. Kim, G. Jorge, and A. P. Ramirez, cond-mat/0510386 (2005).

[6] N. Hur, S. Park, S. Guha, A. Borissov, V. Kiryukhin, and S-W. Cheong, Appl. Phys. Lett. **87**, 042901 (2005).

[7] C. de la Cruz, F. Yen, B. Lorenz, Y. Q. Wang, Y. Y. Sun, M. M. Gospodinov, and C. W. Chu, Phys. Rev. B **71**, 060407(R) (2005).

[8] B. Lorenz, A. P. Litvinchuk, M. M. Gospodinov, and C. W. Chu, Phys. Rev. Lett. **92**, 087204 (2004).

[9] T. Goto, T. Kimura, G. Lawes, A. P. Ramirez, and Y. Tokura, Phys. Rev. Lett. **92**, 257201 (2004).

[10] N. Hur, S. Park, P. A. Sharma, S. Guha, and S-W. Cheong, Phys. Rev. Lett. **93**, 107207 (2004).

[11] G. Lawes, A. P. Ramirez, C. M. Varma, and M. A. Subramanian, Phys. Rev. Lett. **91**, 257208 (2003).

[12] N. S. Rogado, J. Li, A. W. Sleight, and M. A. Subramanian, Adv. Mater. **17**, 2225 (2005).

[13] M. Saito, R. Higashinaka, and Y. Maeno, Phys. Rev. B **72**, 144422 (2005)

[14] M. A. Subramanian, T. He, J. Chen, N. S. Rogado, T. G. Calvarese, and A. W. Sleight, Adv. Mater. **18**, 1737 (2006).

[15] R. C. Rai, J. Cao, J. L. Musfeldt, D. J. Singh, X. Wei, R. Jin, Z. X. Zhou, B. C. Sales, and D. Mandrus, Phys. Rev. B **73**, 075112 (2006).

[16] Z.-T. Zhu, J. L. Musfeldt, Z. S. Teweldemedhin, and M. Greenblatt, Phys. Rev. B **65**, 214519 (2002).

[17] F. Wooten, *Optical Properties of Solids* (Academic Press, New York, 1972).

[18] J. Cao, J. T. Haraldsen, R. C. Rai, S. Brown, J. L. Musfeldt, Y. J. Wang, X. Wei, M. Apostu, R. Suryanarayanan, and A. Revcolevschi, Phys. Rev. B **74**, 045113 (2006).

[19] D. J. Singh and L. Nordstrom, *Planewaves, Pseudopotentials and the LAPW Method, 2nd Ed.* (Springer, Berlin, 2006).

[20] D. Singh, Phys. Rev. B **43**, 6388 (1991).

[21] P. Blaha, K. Schwarz, G. K. H. Madsen, D. Kvasnicka, and J. Luitz, WIEN2K, 2002, *an Augmented Plane Wave + Local Orbitals Program for calculating crystal properties* (Karlheinz Schwarz, Technische Universitat Wien, Austria).

[22] E. Sjostedt, L. Nordstrom, and D. J. Singh, Solid State Commun. **114**, 15 (2000).

[23] Here we used an effective $U - J = 5$ eV, $J = 0$, though because of the fully spin polarized nature of the Ni the results would not depend on the choice of J provided $U - J$ is held constant.

[24] G. A. Sawatzky and J. W. Allen, Phys. Rev. Lett. **53**, 2339 (1984).

[25] J. Schnack, M. Brüger, M. Luban, P. Kögerler, E. Morosan, R. Fuchs, R. Modler, H. Nojiri, R. C. Rai, J. Cao, and J. L. Musfeldt, Phys. Rev. B, **73**, 094401 (2006).

[26] T. Ido, K. Magoshi, H. Eisaki, and S. Uchida, Phys. Rev. B **44**, 12094 (1991).

[27] R. Juza, H. Seidel, and J. Tiedemann, Angew. Chem. Internat. Edit. **5**, 85 (1966).

[28] Although magneto-optical measurements below 0.75 eV are limited by the energy range (0.75 - 4.1 eV) of our experimental set-up, we suspect that splitting of Ni(cross-tie) d to d excitation may be similar to the splitting of Ni (spine) d to d excitation.

[29] A. F. García-Flores, E. Granado, H. Martinho, R. R. Urbano, C. Rettori, E. I. Golovenchits, V. A. Sanina, S. B. Oseroff, S. Park, and S-W. Cheong, Phys. Rev. B **73**, 104411 (2006).

[30] D. Wang, J. Tang, Z. Zou, and J. Ye, Chem. Mater. **17**, 5177 (2005).

[31] K. Terakura, A. R. Williams, T. Oguchi, and J. Kübler, Phys. Rev. Lett. **52**, 1830 (1984).

[32] R. Merlin, Phys. Rev. Lett. **54**, 2727 (1985)

[33] M. R. Norman and A. J. Freeman, Phys. Rev. B **33**, 8896 (1986).

[34] V. I. Anisimov, M. A. Korotin, and E. Z. Kurmaev, J. Phys. Condens. Matter **2**, 3973 (1990).

[35] V. I. Anisimov, J. Zaanen, O. K. Andersen, Phys. Rev. B **44**, 943 (1991).

[36] A. Svanne and O. Gunnarsson, Phys. Rev. Lett. **65**, 1148 (1990).

[37] M. Arai and T. Fujiwara, Phys. Rev. B **51**, 1477 (1995).

[38] D. Kodderitzsch, W. Hergert, W. M. Temmerman, Z. Szotek, A. Ernst, and H. Winter, Phys. Rev. B **66**, 064434

(2002).
[39] F. Aryasetiawan and O. Gunnarsson, Phys. Rev. Lett. **74**, 3221 (1995).
[40] S. Massidda, A. Continenza, M. Posternak, and A. Baldereschi, Phys. Rev. B **55**, 13494 (1997).
[41] J. L. Li, G. M. Rignanese, and S. G. Louie, Phys. Rev. B **71**, 193102 (2005).
[42] I. D. Brown, *Structure and Bonding in Crystals* (Academic Press, New York, 1981).
[43] J.D. Woodward, J. Choi, J.L. Musfeldt, J.T. Haraldsen, X. Wei, H.-J. Koo, D. Dai, M.-H. Whangbo, C.P. Landee, and M.M. Turnbull, Phys. Rev. B. **71**, 174416 (2005).
[44] J. Choi, J.D. Woodward, J.L. Musfeldt, X. Wei, J. He, R. Jin, and D. Mandrus, Phys. Rev. B. **70**, 085107 (2004).
[45] A. B. Sushkov, O. Tchernyshyov, W. Ratcliff II, S. W. Cheong, and H. D. Drew, Phys. Rev. Lett. **94**,137202 (2005).
[46] S.-H. Lee, C. Broholm, W. Ratcliff, G. Gasparovic, Q. Huang, T. H. Kim, and S.-W. Cheong, Nature **418**, 856 (2002).
[47] W. Ratcliff II, V. Kiryukhin, M. Kenzelmann, S.-H. Lee, R. Erwin, J. Schefer, N. Hur, S. Park, and S-W. Cheong, Phys. Rev. B **72**, 060407(R) (2005).
[48] G. R. Blake, L. C. Chapon, P. G. Radaelli, S. Park, N. Hur, S-W. Cheong, and J. Rodríguez-Carvajal, Phys. Rev. B **71**, 214402 (2005).